Modelling of mid-infrared interferometric signature of hot exozodiacal dust emission

Florian Kirchschlager,[1,2]* Sebastian Wolf,[2] Robert Brunngräber,[2] Alexis Matter,[3] Alexander V. Krivov[4] and Aaron Labdon[5]

[1]*Department of Physics and Astronomy, University College London, Gower Street, London WC1E 6BT, UK*
[2]*Institute of Theoretical Physics and Astrophysics, Kiel University, Leibnizstraße 15, D-24118 Kiel, Germany*
[3]*Laboratoire Lagrange, Université Côte d'Azur, Observatoire de la Côte d'Azur, CNRS, Boulevard de l'Observatoire, CS 34229, F-06304 Nice Cedex 4, France*
[4]*Friedrich Schiller University Jena, Astrophysical Institute and University Observatory, Schillergäßchen 2-3, D-07745 Jena, Germany*
[5]*Department of Physics and Astronomy, University of Exeter, Stocker Road, Exeter EX4 4QL, UK*

ABSTRACT

Hot exozodiacal dust emission was detected in recent surveys around two dozen main-sequence stars at distances of less than 1 au using the *H*- and *K*-band interferometry. Due to the high contrast as well as the small angular distance between the circumstellar dust and the star, direct observation of this dust component is challenging. An alternative way to explore the hot exozodiacal dust is provided by mid-infrared interferometry. We analyse the *L*, *M* and *N* bands interferometric signature of this emission in order to find stronger constraints for the properties and the origin of the hot exozodiacal dust. Considering the parameters of nine debris disc systems derived previously, we model the discs in each of these bands. We find that the *M* band possesses the best conditions to detect hot dust emission, closely followed by *L* and *N* bands. The hot dust in three systems – HD 22484 (10 Tau), HD 102647 (β Leo) and HD 177724 (ζ Aql) – shows a strong signal in the visibility functions, which may even allow one to constrain the dust location. In particular, observations in the mid-infrared could help to determine whether the dust piles up at the sublimation radius or is located at radii up to 1 au. In addition, we explore observations of the hot exozodiacal dust with the upcoming mid-infrared interferometer Multi AperTure mid-Infrared SpectroScopic Experiment (MATISSE) at the Very Large Telescope Interferometer.

Key words: techniques: interferometric – interplanetary medium – circumstellar matter – infrared: planetary systems.

1 INTRODUCTION

Hot exozodiacal dust is located at the closest possible distances to main-sequence stars (Absil et al. 2006). Due to its high temperature the dust is traced in observations in the near-infrared (e.g. Akeson et al. 2009; Defrère et al. 2011). According to the sparing amount of exozodiacal dust in circumstellar environments, the emitted fluxes are quite low, and the excesses above the stellar photospheres are marginal. Therefore, detection of circumstellar emission caused by exozodiacal dust was so far only possible through interferometric observations (Absil et al. 2013; Ertel et al. 2014; Nunez et al. 2017).

Based on near- and mid-infrared (NIR and MIR, respectively) observations of a sample of nine debris disc systems harbouring hot exozodiacal dust, Kirchschlager et al. (2017) constrained the dust properties and dust distribution in the vicinity of these stars. The dust was found to be located within ∼0.01–1 au, and the exozodiacal dust masses amounted to $(0.2-3.5) \times 10^{-9} \, M_\oplus$. The dust grains were determined to be below 0.2–0.5 μm.

The origin of the hot exozodiacal dust is still highly debated and explaining the presence of small dust grains located close to the star in sufficient large amount over a long time is challenging. Proposed scenarios are the aftermath of a large collision or heavy bombardment, dynamically perturbed comets, planetesimals or planets, which move and disintegrate in the inner system, the sublimation of a supercomet close to the star, an inward drift of dust grains caused by the Poynting–Robertson drag, as well as charged nanoscale dust

* E-mail: f.kirchschlager@ucl.ac.uk

Table 1. Parameters of targets with NIR excess observed with VLTI/VINCI (Absil et al. 2009) and CHARA/FLUOR (Absil et al. 2013), which is attributed to circumstellar dust.

HD number	HIP number	Alter. name	d (pc)	$T_\star$ (K)	$L_\star$ ($L_\odot$)	Spectral class	Age (Gyr)	R (au)	M_{dust} (10^{-9} M$_\oplus$)	a_{max} (μm)
10700	8102	τ Cet	3.7	5290	0.46	G8 V	10	0.016–0.056	0.03–0.14	0.42
22484	16852	10 Tau	13.7	5998	3.06	F9 IV-V	6.7	0.039–0.49	0.38–6.95	0.71
56537	35350	λ Gem	28.9	7932	27.4	A3 V	0.5	0.12–0.65	0.69–3.1	0.42
102647	57632	β Leo	11.1	8604	13.25	A3 V	0.1	0.08–0.98	0.57–5.7	0.77
172167	91262	α Lyr	7.8	9620	37	A0 V	0.7	0.15–0.65	0.89–3.5	0.35
177724	93747	ζ Aql	25.5	9078	36.56	A0 IV-V	0.8	0.14–1.0	1.79–10.2	0.51
187642	97649	α Aql	5.1	7680	10.2	A7 IV-V	1.3	0.09–0.11	0.84–1.0	0.2
203280	105199	α Cep	15.0	7700	19.97	A7 IV-V	0.8	0.11–0.43	0.54–2.1	0.35
216956	113368	α PsA	7.7	8590	16.6	A3 V	0.4	0.11–0.17	0.12–0.2	0.25

References. The distances are derived from parallax measurements (van Leeuwen 2007). Stellar temperatures and luminosities are adopted from Habing et al. (2001); van Belle et al. (2001); van Belle et al. (2006); Müller, Löhne & Krivov (2010); Zorec & Royer (2012); and Boyajian et al. (2013); spectral classes and stellar ages from Mamajek (2012); Vican (2012) and Absil et al. (2013), and disc and dust constraints are from Kirchschlager et al. (2017).

grains trapped in a stellar magnetic field (Kral et al. 2017, and references therein). However, each attempt to explain the presence of hot exozodiacal dust suffers from inconsistencies. Therefore, further observations are necessary to shed light on the properties of the hot dust.

While photometry of the dust emission at wavelengths below 15 μm suffers from the uncertainty due to small fluxes compared to the stellar spectrum, interferometric observations provide a direct estimation of the flux ratio between the circumstellar environment and the stellar photosphere. Well determined NIR and MIR fluxes are necessary to place tighter constraints on the parameters of the hot exozodiacal dust. Therefore, complementary interferometric observations in this wavelength range are required.

MATISSE (Multi AperTure mid-Infrared SpectroScopic Experiment; Lopez et al. 2014) is an upcoming second generation Very Large Telescope Interferometer (VLTI) instrument, which will offer simultaneous four-beam interferometry and spectroscopic capabilities in the L ($\lambda = 2.8$–4.0 μm), M (4.5–5.0 μm) and N bands (8–13 μm). Especially, the new possibility of interferometric observations in the L and M bands will improve and complete the investigation of milliarcsecond scale MIR emission (Matter et al. 2016a).

In this paper, we investigate the MIR interferometric signature of hot exozodiacal dust emission around nine main-sequence stars. For this purpose, we use model parameters derived by Kirchschlager et al. (2017), calculate thermal reemission and scattered light maps and derive the corresponding visibility functions. The applied disc and dust models are described in Section 2 and the results are presented in Section 3. In Section 4, we summarize our findings and have an outlook on observations of hot exozodiacal dust with the upcoming instrument MATISSE.

2 STELLAR SAMPLE AND MODEL

In this section, we present the strategy to model and evaluate the interferometric signature of the exozodiacal dust belt in the nine selected systems. The investigated sample of systems is introduced in Section 2.1 and the applied model is described in Section 2.2. In Section 2.3, the procedure to simulate visibility functions of these systems is given.

2.1 Stellar sample

In Table 1, those debris disc systems are compiled that show a significant NIR excess in the K band (1.59–1.77 μm), which is indicative of hot exozodiacal dust (VLTI/VINCI, Absil et al. 2009; CHARA/FLUOR, Absil et al. 2013). In addition, interferometric flux measurements at $\lambda \approx 10$ μm (Mennesson et al. 2014) exist for these systems, which strongly constrain the disc and dust parameters (Kirchschlager et al. 2017). All of these stars are on or close to the main sequence, with spectral classes ranging from G8 to A0 and luminosities from $L_\star \sim 0.4$ L$_\odot$ up to ~ 40 L$_\odot$. The stellar fluxes are in the range of 20–263 Jy and 3–39 Jy for the L and N bands, respectively.

2.2 Model description

For the sake of conformity, we use the same simple model as in Kirchschlager et al. (2017).

Disc properties: The disc model consists of a thin, radially symmetric ring with an inner radius R and outer radius of $1.5\,R$. The number density decreases with distance as $n(r) \propto r^{-1}$. The disc is assumed to be face-on ($i = 0°$) and the half opening angle amounts to 5°.

Dust properties: Each dust ring is composed of compact, spherical dust grains with grain radius a. The grains are assumed to consist of pure graphite ($\rho = 2.24$ g cm^{-3}; Weingartner & Draine 2001), using the 1/3–2/3 approximation (Draine & Malhotra 1993). Silicate compositions could be excluded by the modelling of Kirchschlager et al. (2017), since the presence of the prominent silicate feature at ~ 10.0 μm would contradict the observed MIR fluxes.

Kirchschlager et al. (2017) showed that the grain radii of the hot exozodiacal dust in most of the systems must be below 0.5 μm. However, in the case of HD 10700 (τ Cet), HD 22484 (10 Tau) and HD 56537 (λ Gem), the presence of micrometer-sized grains cannot be ruled out, since only MIR observations (Mennesson et al. 2014) with a limited resolution are available for these systems. Nevertheless, we expect that micrometer-sized grains are absent in these systems, too. We estimate the maximum grain size in these three systems by extrapolating the steepest part of the blue–red border, around point C, to larger sizes (see Fig. 1 for the system HD 22484).

As shown in Fig. 1 (adopted from Kirchschlager et al. 2017), there exists an area in the parameter space (a, R) in which the
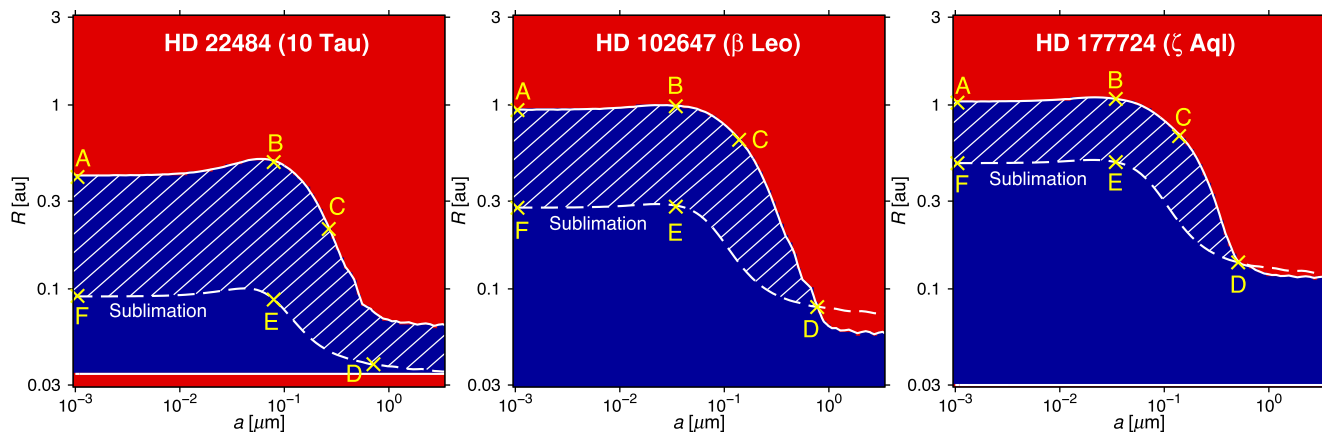
Figure 1. Parameter space explored for the systems HD 22484, HD 102647 and HD 177724 (Kirschschlager et al. 2017). Blue regions correspond to models, which possess simulated NIR and MIR fluxes, which are consistent to previous observations within their errors, red regions fail. The shaded areas correspond to parameter settings that allow the existence of hot exozodiacal dust, and which are constrained by observational data (blue–red border, white solid line) and the sublimation radius (white dashed line). The configurations A–F are the extremes of the model space selected for the visibility calculations.

models can reproduce previous observations[1] in the NIR (VLTI/VINCI, FLUOR/CHARA; Absil et al. 2009, 2013) and MIR (Keck; Mennesson et al. 2014) while the dust is still not sublimated. Details for the calculation of the sublimation radius are given in Kirschschlager et al. (2017). While the analysis of the entire parameter space would result in extensive data, we instead explore our simulations for each system at six representative parameter configurations (A–F) at the various borders of the possible parameter range, enabling to study the impact of individual parameters on the visibility functions with an appropriate computational effort. The corresponding grain size a, disc ring radius R and the dust mass M_{dust} of each configuration are used for the modelling of the individual systems. The configurations A, B and C correspond to larger disc extensions and higher dust masses than the configurations D, E and F that are defined by the sublimation radius. The grain size increases in the alphabetical order from configuration A to D, and then decreases to configuration F. In Table 2, we list the parameter settings for the systems HD 22484, HD 102647 and HD 177724.

2.3 Procedure and software applied

The optical properties of the grains are calculated with the software tool MIEX, which is based on the Mie scattering theory (Mie 1908; Wolf & Voshchinnikov 2004). For each parameter configuration (A–F), single scattering and reemission simulations are performed and the maps are calculated using an enhanced version of the tool DEBRIS (Ertel et al. 2011). The simulations are performed in the L ($\lambda = 3.5\,\mu m$), M (4.7 μm) and N bands (10.0 μm).

Subsequently, the brightness distributions are integrated along one direction in the disc and the visibility functions are derived along the perpendicular direction. Using the Van Cittert–Zernike theorem, the intensity map is used to determine the visibility of the system via Fourier transformation as a function of projected telescope baseline length.

In addition, for each of the nine systems, we calculate the visibility function $V_\star$ of the single star only. We determine the difference $\Delta V = V_\star - V_{(\star + disc)}$ of the visibility functions of the single star

[1] In this area of the parameter space, the models are consistent with the observational data within their error bars (Kirschschlager et al. 2017).

Table 2. Parameters of the configurations A–F corresponding to the acceptable parameter space (Fig. 1) for the systems HD 22484, HD 102647 and HD 177724.

		A	B	C	D	E	F
HD 22484							
R	(au)	0.41	0.49	0.21	0.04	0.09	0.09
a	(μm)	0.001	0.079	0.266	0.712	0.079	0.001
M_{dust}	($10^{-9}\,M_\oplus$)	6.94	6.72	3.62	1.23	0.38	0.53
HD 102647							
R	(au)	0.94	0.98	0.65	0.08	0.28	0.28
a	(μm)	0.001	0.034	0.138	0.77	0.034	0.001
M_{dust}	($10^{-9}\,M_\oplus$)	5.73	5.66	5.17	0.57	0.7	0.75
HD 177724							
R	(au)	1.03	1.08	0.68	0.14	0.49	0.48
a	(μm)	0.001	0.034	0.138	0.509	0.034	0.001
M_{dust}	($10^{-9}\,M_\oplus$)	10.1	10.2	9.04	1.79	3.09	3.23

and the one of the system consisting of star and disc at baseline lengths of 20–140 m. When the difference ΔV is significant, the visibilities $V_{(\star + disc)}$ and $V_\star$ are directly connected to the flux ratio f between disc and central star via $V_{(\star + disc)} \approx (1 - f)V_\star$ (Di Folco et al. 2004). Therefore, the flux emitted by the dust in the wavebands can be derived by the detection of a significant visibility deficit.

3 RESULTS

In this section, the results of the calculated visibility functions in the L ($\lambda = 3.5\,\mu m$), M (4.7 μm) and N bands (10.0 μm) are presented. We will see that HD 22484, HD 102647 and HD 177724 are the most promising systems.

3.1 Visibility drop

In five of nine systems of Table 1, the visibility difference amounts to values larger than or equal to 2 per cent (Table 3), namely HD 22484, HD 102647, HD 172167, HD 177724 and HD 187642.

Table 3. Visibility differences ΔV for the simulated interferometric observations in the *M* band and at baseline lengths in the range of 20–140 m. The values for the most promising systems HD 22484, HD 102647 and HD 177724 are highlighted. In general, the values for the *L* and *N* bands are only slightly smaller.

HD number	ΔV at configurations	
	A, B, C (per cent)	D, E, F (per cent)
10700	0.7–1.3	0.2–1.7
22484	**2.5–4.5**	**0.5–∼10**
56537	0.7–1.4	0.2–1.6
102647	**2.5–4**	**0.5–3**
172167	1.5–2	1.2–2.5
177724	**2–3.5**	**2–4.5**
187642	1.5–3.5	1.5–3.5
203280	0.8–1.3	0.4–1.6
216956	0.2–0.4	0.2–0.8

The results of the configurations A, B and C, that correspond to larger disc extensions and higher dust masses, show distinctly higher visibility differences than in the cases for the configurations E and F, that correspond to dust locations close to the sublimation radius. Except for configuration D in HD 22484, the visibility differences are up to 5 per cent in the *L* and *M* bands and 4 per cent in the *N* band. In general, the visibility differences for the *L* and *N* bands are slightly smaller than the ones for the *M* band. For configuration D in HD 22484, the differences are up to ∼10 per cent for both the *L* and *M* bands and 3 per cent in the *N* band.

The hot exozodiacal dust emission in the system of HD 216956 amounts to less than 0.8 per cent and hence constitutes the system with the lowest visibility difference. For the remaining three systems – HD 10700, HD 56537 and HD 203280 – the hot dust emission causes a visibility drop lower than 1.7 per cent.

Overall, these results show that a larger disc ring radius *R* produces a larger visibility deficit, while there is a weaker impact of the dust grain size.

3.2 Constraints for the dust properties

Observations of the systems HD 22484, HD 102647 and HD 177724 potentially allow one to derive constraints for the dust location (Figs 2–4). For these systems, the L and M bands visibility differences between the blue and red curves are larger than or in the order of 1.5 per cent. Using an instrument with a 1σ visibility accuracy of ∼0.5 per cent, the *L* and *M* bands observations provide the possibility to significantly (3σ) distinguish between the configurations A, B, C (larger disc radius) and the configurations E, F (sublimation radius). In other words, one could distinguish between emission from dust grains piled up at the sublimation radius and emission from dust grains located at a ten times larger radial distance. However, configuration D hampers a clear allocation of the location of the dust emission, as the visibility curve of configuration D intersects the blue curves in all three systems in both the L and M bands. For HD 22484 and HD 102647, the *N*-band observations at baselines smaller than 100 and 65 m, respectively, are able to avoid a confusion with configuration D. For HD 177724, however, configuration D cannot be distinguished clearly from configurations that correspond to larger discs extensions. A non-detection of dust emission at baselines longer than 100 m would indicate dust located near to the sublimation radius and grain sizes smaller than 0.7 μm in these three systems.
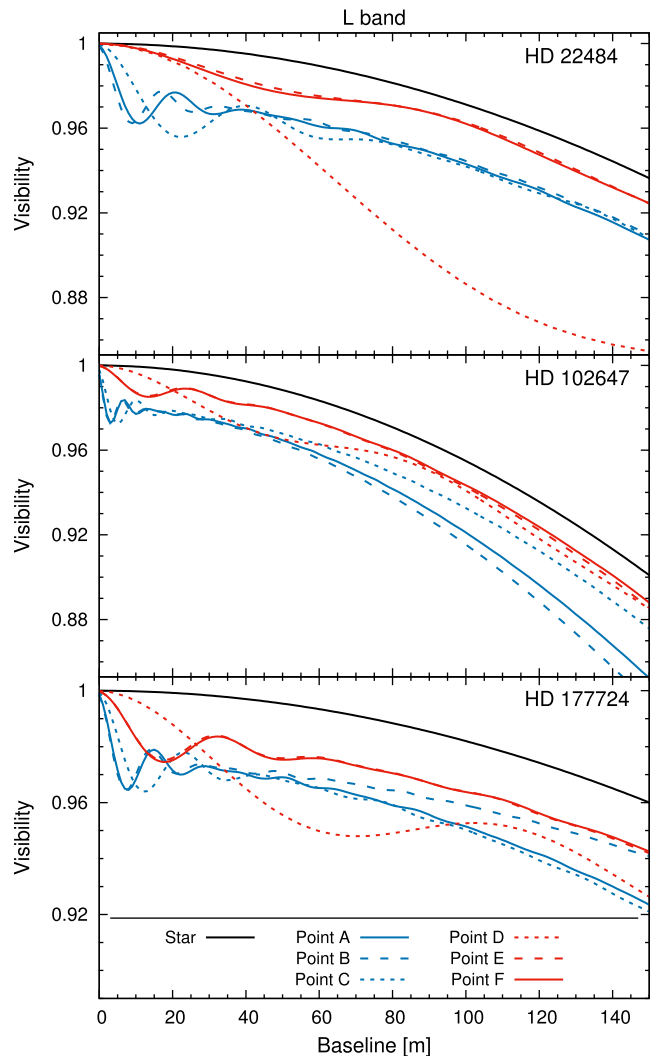

Figure 2. *L* band visibilities ($\lambda = 3.5$ μm) for three systems harbouring exozodiacal dust: HD 22484 (top panel), HD 102647 (middle panel) and HD 177724 (bottom panel). The black solid line indicates the visibility of the central star without disc ($V_\star$). Different configurations in the parameter space (see Fig. 1) are indicated by different colours and line types.

Overall, MIR interferometric observations potentially allow one to constrain the parameters of the hot exozodiacal dust if the 1σ visibility accuracy of the instrument amounts to ∼0.5 per cent.

These constraints might help to reveal the origin of the dust material, which is still highly debated. Kirchschlager et al. (2017) suggested the possibility that the grain temperatures of the exozodiacal dust belts are the same in all systems. We checked that MIR interferometric observations would not be able to confirm or exclude this hypothesis. The possible temperature ranges are too wide to make any further restrictions.

4 CONCLUSIONS AND OUTLOOK

We conclude our study with a summary of the results of MIR interferometric observations of the hot exozodiacal dust belts found in Section 3. Based on constraints of the disc and dust distributions derived in Kirchschlager et al. (2017), we investigated the possibility
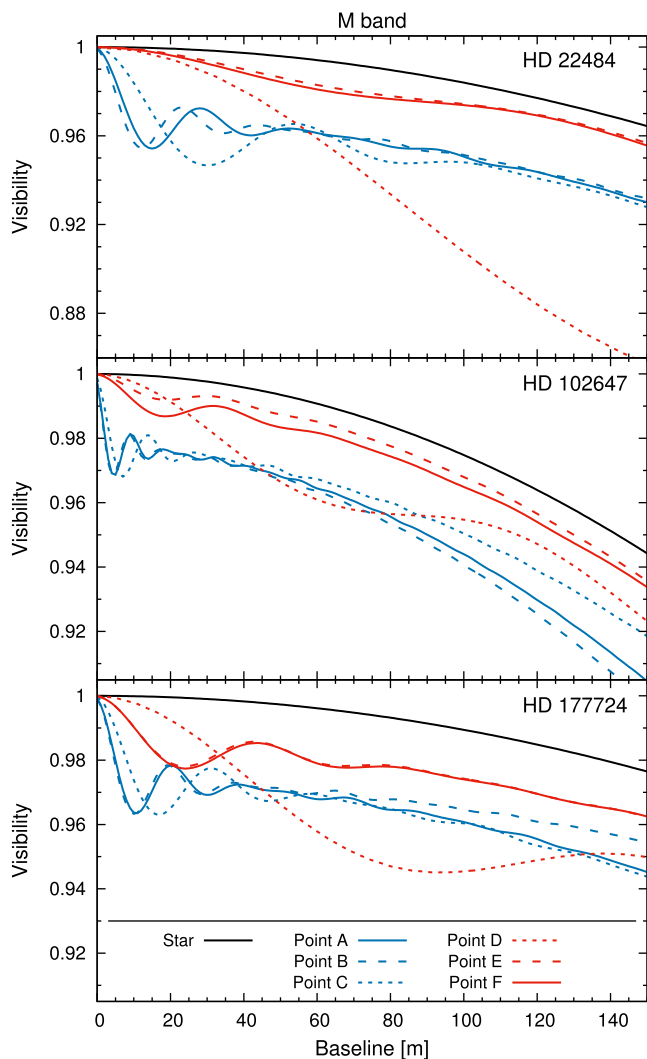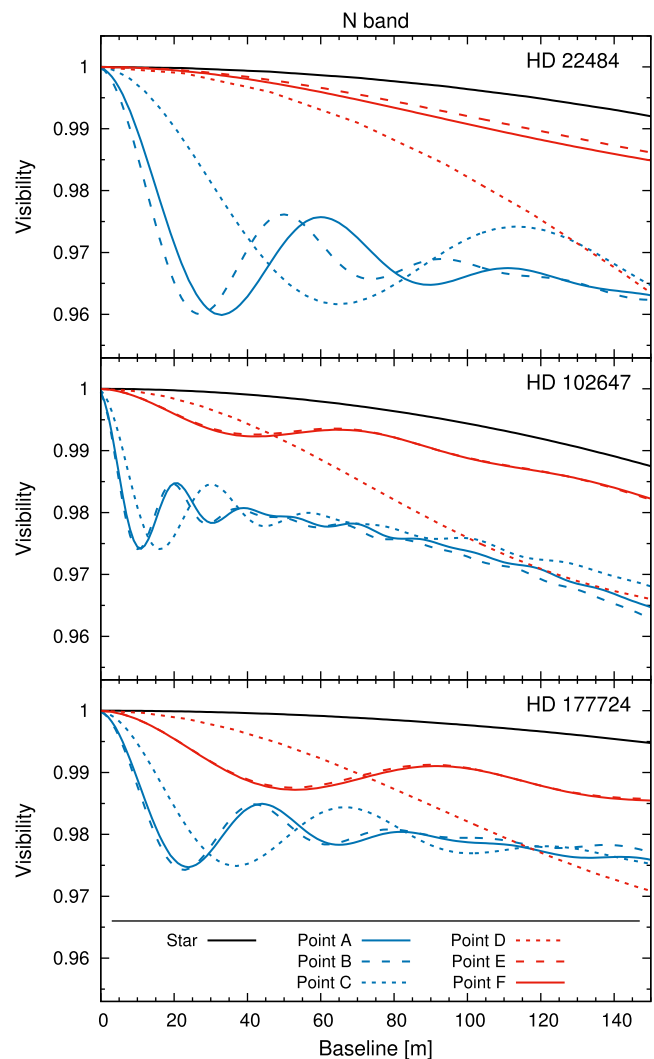
Figure 3. Same as Fig. 2, but for the *M* band (λ = 4.7 μm).

Figure 4. Same as Figs 2 and 3, but for the *N* band (λ = 10 μm).

to detect hot exozodiacal dust emission around nine main-sequence stars using MIR interferometry. Our conclusions are as follows:

(i) The visibility drop caused by the hot exozodiacal dust is in five of the nine systems of Table 1 – HD 22484, HD 102647, HD 172167, HD 177724 and HD 187642 – larger than 2 per cent. In general, the visibility differences for the *L* and *N* bands are slightly smaller than the ones for the *M* band.

(ii) MIR interferometric observations will potentially allow one to constrain the parameters of the hot exozodiacal dust systems and hence might help to reveal the origin of the dust material. Assuming a 1σ visibility accuracy of ∼0.5 per cent, a combination of the *L*, *M* and *N* bands observations has the potential to distinguish between emission of dust grains at the sublimation radius and emission of dust grains located at larger distances. The most promising systems are HD 22484 and HD 102647, followed by HD 177724. Both the detection and the non-detection may help to constrain the dust location.

As an outlook, the upcoming instrument MATISSE at the VLTI will specifically perform simultaneous observations in the *L*, *M* and *N* bands, which would make it a very suitable instrument for the characterization of the hot exozodiacal dust. However, such a study appears challenging for MATISSE given the required visibility

accuracy of less than 1 per cent. Indeed, theoretical MATISSE visibility accuracies of 1 to 3 per cent in *L* and *M* bands, and 8 per cent in the *N* bands, were estimated for a 20 Jy source; estimates were based on SNR calculations including the contribution of the fundamental noises (source photon noise, readout noise, thermal background photon noise) and the transfer function variations (Lopez et al. 2014; Matter et al. 2016b). Nevertheless, in the frame of the recent MATISSE test phase, several lab transfer function measurements were performed over a few hours with a very bright artificial IR source. Such a source would have an equivalent flux, if observed with the UTs, of 20 to 70 Jy in the *N* band, 400 Jy in the *M* band and 600 Jy in the *L* band. This leads to absolute visibility accuracies of 0.5 per cent in the *L* band, 0.4 per cent in the *M* band and less than 2.5 per cent in the *N* band, on average, over the corresponding spectral band. Those promising results are extensively described in internal ESO documents written by the MATISSE consortium (private communication with A. Matter). Eventually, a proper study of the detectability of exozodiacal dust with MATISSE will require a knowledge of its real on-sky performance, which will notably include the effects of the sky thermal background fluctuation, the atmospheric turbulence, or the on-sky calibration. The beginning of the on-sky tests (commissioning) of MATISSE is planned for 2018 March.

ACKNOWLEDGEMENTS

REFERENCES

Absil O. et al., 2006, A&A, 452, 237
Absil O., Mennesson B., Le Bouquin J.-B., Di Folco E., Kervella P., Augereau J.-C., 2009, ApJ, 704, 150
Absil O. et al., 2013, A&A, 555, A104
Akeson R. L. et al., 2009, ApJ, 691, 1896
Boyajian T. S. et al., 2013, ApJ, 771, 40
Defrère D. et al., 2011, A&A, 534, A5
Di Folco E., Thévenin F., Kervella P., Domiciano de Souza A., Coudé du Foresto V., Ségransan D., Morel P., 2004, A&A, 426, 601
Draine B. T., Malhotra S., 1993, ApJ, 414, 632
Ertel S., Wolf S., Metchev S., Schneider G., Carpenter J. M., Meyer M. R., Hillenbrand L. A., Silverstone M. D., 2011, A&A, 533, A132
Ertel S. et al., 2014, A&A, 570, A128
Habing H. J. et al., 2001, A&A, 365, 545
Kirchschlager F., Wolf S., Krivov A. V., Mutschke H., Brunngräber R., 2017, MNRAS, 467, 1614
Kral Q. et al., 2017, Astron. Rev., preprint (arXiv:1703.02540)
Lopez B. et al., 2014, The Messenger, 157, 5
Mamajek E. E., 2012, ApJ, 754, L20
Matter A. et al., 2016a, Proc. SPIE Conf. Ser. Vol. 9907, An Overview of the Mid-Infrared Spectro-Interferometer MATISSE: Science, Concept, and Current Status. SPIE, Bellingham, p. 99070A
Matter A. et al., 2016b, Proc. SPIE Conf. Ser. Vol. 9907, MATISSE: Specifications and Expected Performances. SPIE, Bellingham, p. 990728
Mennesson B. et al., 2014, ApJ, 797, 119
Mie G., 1908, Annalen der Physik, 330, 377
Müller S., Löhne T., Krivov A. V., 2010, ApJ, 708, 1728
Nunez P. D. et al., 2017, A&A, preprint (arXiv:1709.01655)
van Belle G. T., Ciardi D. R., Thompson R. R., Akeson R. L., Lada E. A., 2001, ApJ, 559, 1155
van Belle G. T. et al., 2006, ApJ, 637, 494
van Leeuwen F., 2007, A&A, 474, 653
Vican L., 2012, ApJ, 143, 135
Weingartner J. C., Draine B. T., 2001, ApJ, 548, 296
Wolf S., Voshchinnikov N. V., 2004, Comput. Phys. Commun., 162, 113
Zorec J., Royer F., 2012, A&A, 537, A120

This paper has been typeset from a TeX/LaTeX file prepared by the author.